

# First ground-based optical analysis of $H_{\beta}$ Doppler profiles close to local noon in the cusp

S. C. Robertson<sup>1,2</sup>, B. S. Lanchester<sup>1</sup>, M. Galand<sup>3</sup>, D. Lummerzheim<sup>4</sup>, A. B. Stockton-Chalk<sup>1</sup>, A. D. Aylward<sup>2</sup>, I. Furniss<sup>2</sup>, and J. Baumgardner<sup>5</sup>

<sup>1</sup>Space Environment Physics, University of Southampton, UK

<sup>2</sup>Atmospheric Physics Laboratory, University College London, UK

<sup>3</sup>Space and Atmospheric Physics Group, Imperial College London, UK

<sup>4</sup>Geophysical Institute, University of Alaska, USA

<sup>5</sup>Centre for Space Physics, Boston University, MA, USA

Received: 16 June 2006 – Accepted: 31 August 2006 – Published: 20 October 2006

**Abstract.** Observations of hydrogen emissions along the magnetic zenith at Longyearbyen (78.2N, 15.8E geographic) are used to investigate the energy and source of protons precipitating into the high latitude region. During the hours around local solar noon (11:00 UT), measurements of the hydrogen Balmer  $\beta$  line are severely affected by sunlight, such that most data until now have been disregarded during these times. Here we use a simple technique to subtract sunlight contamination from such spectral data. An example is shown in which the removal of twilight contamination reveals a brightening of  $H_{\beta}$  aurora over Svalbard on 27 November 2000 between 08:00 UT and 10:00 UT, which is centred on magnetic noon (08:48 UT). These data were measured by the High Throughput Imaging Echelle Spectrograph (HiTIES), one instrument on the Southampton-UCL Spectrographic Imaging Facility (SIF). Data from the IMAGE satellite confirms the location of a cusp “spot” over Svalbard at the time of the ground-based measurements, which moved in response to changes in the IMF conditions. A coincident pass of the DMSP F12 satellite provided input spectra for modelling studies of the  $H_{\beta}$  profiles, which confirm that the method for removing the twilight contamination is robust. The results described here are the first ground-based optical measurements of  $H_{\beta}$  Doppler profiles from the cusp region close to local solar noon, when scattered sunlight swamps the raw data.

formation about the processes that protons undergo as they propagate through the upper atmosphere (e.g. Lummerzheim and Galand, 2001). In particular, spectrographic measurements using CCD detectors allow the whole wavelength range of the Doppler shifted profile of H emissions to be recorded simultaneously. Given sufficient wavelength resolution (0.13 nm herein), these profiles can be combined with modelling studies to determine the energy spectrum and energy flux of the incoming hydrogen, and hence gain insight into the source of the protons (Galand and Chakrabarti, 2006).

There is particular interest in the emissions resulting from proton precipitation in the region of the cusp, where these emissions are the unique signature of protons that have gained direct access to the Earth’s ionosphere along newly reconnected field lines at the magnetopause. It should be noted that protons are more suitable than electrons for providing information on solar wind-magnetosphere coupling, as they are less sensitive than electrons to magnetospheric processes, and retain information on their source. The temporal and spatial variations of H emissions in the region in or near the cusp have been highlighted in the many results in recent years from the Spectrographic Imager (SI12)/FUV instrument on the Imager for Magnetopause-to-Aurora Global Exploration (IMAGE) satellite, which provides 5–10 s images of the Doppler-shifted integrated Lyman- $\alpha$  emission at 2 min intervals of the entire auroral oval (Mende, 2000). This emission, like the Doppler-shifted  $H_{\beta}$  emission, is produced solely by proton precipitation into the atmosphere. In a statistical survey of cusp aurora, Frey et al. (2002) used IMAGE data to study the behaviour of a region of intense Lyman- $\alpha$  emission poleward of the oval, making estimates of both the electron and proton energy fluxes at the times of occurrence of the “spot”. As the SI12 does not provide spectral information, the estimate of proton flux is limited by the choice made for the energy of the incident protons. While the spatial

## 1 Introduction

Auroral hydrogen emissions are the spectroscopic signature of energetic proton precipitation into the atmosphere. Hydrogen line profiles measured from the ground provide in-

*Correspondence to:* B. S. Lanchester  
(bsl@phys.soton.ac.uk)

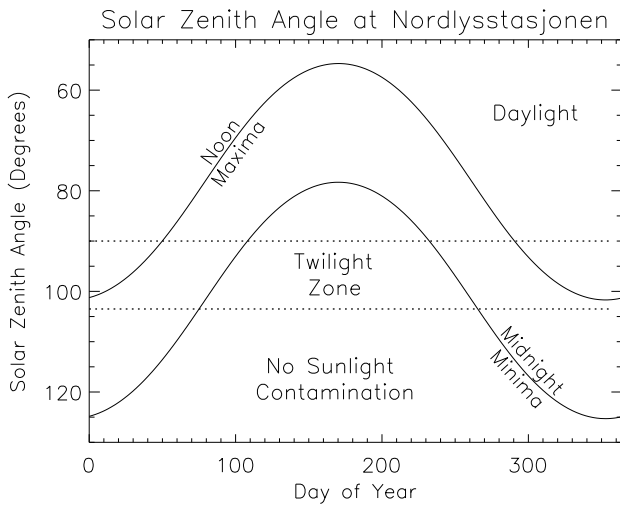


**Fig. 1.** The solar zenith angle (SZA) at Nordlysstasjonen over a year at noon (upper curve) and midnight (lower curve). The two horizontal dotted lines give the SZA range  $90^\circ$  to  $103.5^\circ$  over which twilight contamination is observed.

resolution of this instrument is low (50 km) compared with ground based measurements, it provides an invaluable measure of the magnetospheric context within which to place high resolution spectrographic observations.

Ground-based measurements of hydrogen emissions in the region of the cusp have long been made from Svalbard ( $75^\circ$  magnetic latitude). Ebert–Fastie spectrophotometers scanning over wavelength in time were used to study hydrogen line profiles by Henriksen et al. (1985); Sigernes et al. (1994); Sigernes (1996); Lorentzen et al. (1998) and Deehr et al. (1998). However, as detailed by Henriksen et al. (1985), the effects of Rayleigh scattering are a limiting factor for dayside optical observations, especially for the  $H_\beta$  line. All the above published measurements of hydrogen emissions near local noon are of the  $H_\alpha$  line, which suffers less from Rayleigh scattering because of the  $\lambda^{-4}$  dependence. Henriksen et al. (1985) show examples of zenith spectra taken 3 h before local noon in late January at Svalbard, in the wavelength regions around both the  $H_\alpha$  and  $H_\beta$  lines during an exceptionally strong proton aurora. The  $H_\alpha$  spectrum shows a clear line profile, but the  $H_\beta$  spectrum is dominated by the Fraunhofer absorption line. Henriksen et al. (1985) concluded that there is a significant contribution from Rayleigh scattered sunlight on zenith observations of both  $H_\alpha$  and  $H_\beta$  at solar depression angles less than approximately  $10^\circ$  and  $13^\circ$ , respectively.

The advent of CCD detectors into the field of spectroscopy has provided the means to increase sensitivity as well as resolution in wavelength and time. Such imaging spectrographs are currently the optimal instruments for high spectral resolution measurements of auroral hydrogen lines

(Baumgardner et al., 1993). The High Throughput Imaging Echelle Spectrograph (HiTIES), the main instrument on the Spectrographic Imaging Facility (SIF) in Nordlysstasjonen on Svalbard is well documented (Chakrabarti et al., 2001; McWhirter et al., 2003; Lanchester et al., 2003; Galand et al., 2004). Nordlysstasjonen is located at geographic  $78.2^\circ\text{N}$  and  $15.8^\circ\text{E}$ , which corresponds to a local noon at 10:56:48 UT. At this latitude, the Sun is below the horizon between 27 October and 15 February. Between 14 November and 29 January the Sun does not rise higher than  $6^\circ$  below the horizon, and daytime measurements are possible. However, twilight contamination around local noon can be up to three orders of magnitude brighter than the proton induced aurora. Figure 1 shows the solar zenith angle from Nordlysstasjonen over a year. Twilight emission is detected in HiTIES measurements between solar zenith angles  $90^\circ$  and  $103.5^\circ$ , marked in the figure to delineate times of direct sunlight, twilight, and night. This diagram shows that even at mid-winter, several hours of auroral observation time are severely affected each day by twilight contamination.

In this paper we have applied a simple method to remove the effects of twilight from measured  $H_\beta$  profiles. This method is described in Sect. 2 and applied to H emission Doppler profiles acquired from the HiTIES spectrograph from Svalbard near local noon. A case study of proton induced aurora on 27 November 2000 is presented in Sect. 3. The subtraction method reveals a significant region of underlying  $H_\beta$  emissions, which changed temporally and spatially in response to changes in the solar wind. Measurements from the ACE and IMAGE satellites are used to place the ground-based measurements in the context of the large-scale events. In Sect. 4, energy spectra from the DMSP F12 satellite are used as input to modelling, in order to compare the shape of the  $H_\beta$  profiles that are extracted from the twilight-contaminated data with those produced by the model.

## 2 Twilight contamination

As seen in Fig. 1 there is contamination from sunlight around local noon even at midwinter. The twilight contamination in HiTIES data can be written as

$$T(\lambda) = S_T(\lambda) + A_T(\lambda) \quad (1)$$

where ( $S_T$ ) is Rayleigh scattered sunlight and ( $A_T$ ) is made up of other minor atmospheric emissions. Most of the contamination is scattered sunlight, given by

$$S_T(\lambda) = F(\lambda) \times \sigma_R(\zeta) \quad (2)$$

where  $F(\lambda)$  is the Fraunhofer spectrum,  $\zeta$  is solar zenith angle, and  $\sigma_R$  is the Rayleigh scattering function, inversely proportional to  $\lambda^4$ . Wavelength dependent effects are considered negligible over the 4 nm filter range.

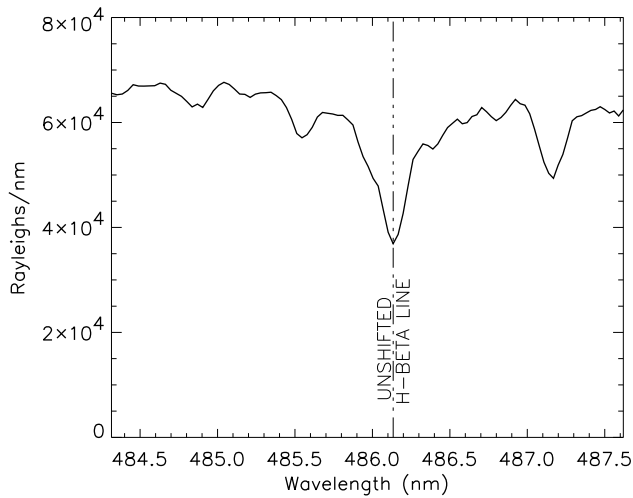


**Fig. 2.** Spectrum ( $T(\lambda)$ ) recorded by HiTIES between 08:45 UT and 10:01 UT on 30 November 2002.

The smaller secondary component is atmospheric emission from a number of sources:

$$A_T(\lambda) = A_{SD}(\lambda) + A_{SI}(\lambda) + C(\lambda) + P(\lambda) \quad (3)$$

where  $A_{SD}(\lambda)$  is from direct sunlight excitation,  $A_{SI}(\lambda)$  is from scattered sunlight and secondary emission due to  $A_{SD}(\lambda)$  emission,  $C(\lambda)$  is emission due to atmospheric chemistry and  $P(\lambda)$  is emission resulting from auroral excitation. These emissions exist over the whole HiTIES spectrum, and have a range of radiative lifetimes. Modelling  $A_T(\lambda)$  is made difficult by lack of experimental results on the minor atmospheric emission species. The auroral  $H_\beta$  line lies between 483 nm and 487 nm. We here assume that  $A_T(\lambda)$  does not vary with wavelength over this range, but varies directly with solar input, such that

$$A_T(\lambda) = A(\zeta) \quad (4)$$

This assumes no long radiative lifetime or chemically driven emissions are present in the band, which is not contradicted by the data. This approximation also assumes there are no auroral emissions other than  $H_\beta$  in the band. Therefore

$$T(\lambda) = F(\lambda) \times \sigma_R(\zeta) + A(\zeta) \quad (5)$$

The overall shape of the twilight contamination spectrum does not vary, but its magnitude varies as a function of  $\zeta$  and atmospheric opacity. The shape of the atmospheric spectrum during twilight is shown in Fig. 2. No auroral emission was detected by the instruments at Nordlysstasjonen during the integration period of this spectrum (08:45 UT to 10:01 UT on 30 November 2000). The twilight brightness, including the effect of atmospheric opacity, is now estimated by normalising the solar spectrum to the background emission level of the data spectrum. The wavelength range selected as the

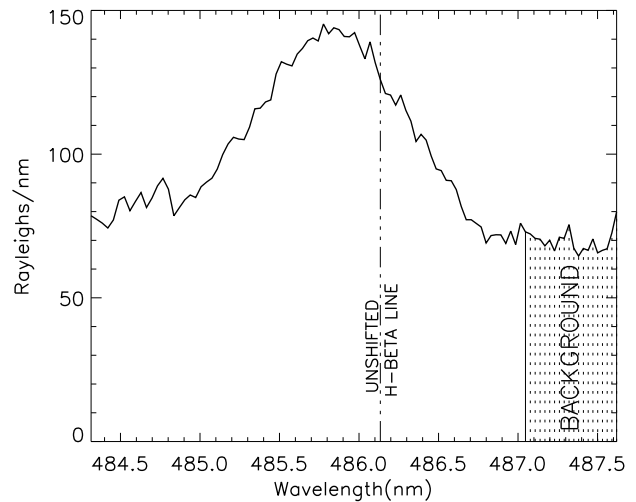


**Fig. 3.** An example Hydrogen  $\beta$  profile. The shaded area indicates the chosen background region of the spectrum.

background area in the  $H_\beta$  filter,  $\bar{\Omega}$ , is shown in Fig. 3, which is a data sample taken when there was no daylight contamination. This shows that the background is well clear of the  $H_\beta$  red wing. The normalising factor is therefore given by

$$\phi = \frac{\bar{\Omega}_D}{\bar{\Omega}_T} \quad (6)$$

where  $\bar{\Omega}_D$  is the background brightness level of the data spectrum, and  $\bar{\Omega}_T$  is the background brightness level of the reference twilight spectrum. Note that maximising the wavelength range over which the background is measured minimises the error in  $\phi$ . At the time that these data were taken, the wavelength range selected for the filter gave the red wing of the  $H_\beta$  line good clearance at the high wavelength end, and hence a good background sample range.

Taking a twilight contaminated data spectrum,  $D(\lambda)$ , the twilight can be estimated using the reference twilight spectrum  $T(\lambda)$  and the scaling constant  $\phi$  (Eq. 6). This estimate can then be subtracted from  $D(\lambda)$  to reveal the underlying spectrum ( $R(\lambda)$ ).

$$R(\lambda) = D(\lambda) - \phi T(\lambda) \quad (7)$$

Figures 4–6 show examples of the twilight estimation process and the resulting subtracted spectra. These will be discussed in more detail in Sect. 3. The process estimates and subtracts  $T(\lambda)$  accurately, to reveal the much smaller underlying hydrogen profile,  $R(\lambda)$ . Note that  $R(\lambda)$  still has the Poisson variance of the larger initial spectrum after the subtraction.

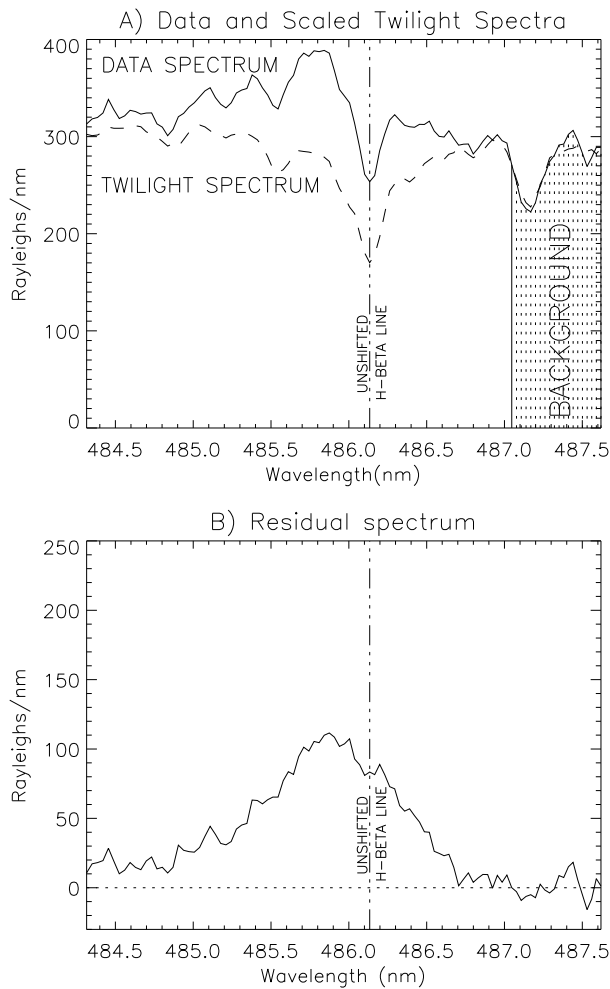


**Fig. 4.** (A) A measured spectrum (solid line), integrated for 60 s beginning at 09:06:34 on 27 November, 2000. The  $\phi$ -scaled twilight spectrum is drawn as a dashed line. (B) The residual spectrum after the scaled twilight spectrum has been subtracted from the data spectrum.

### 3 Observations

#### 3.1 Overview

The present observations were made following a period of exceptional solar activity, with eruptions of four halo Coronal Mass Ejections (CMEs) within 18 h on 24–25 November, 2000. On 27 November 2000, the solar wind velocity was raised ( $\approx 600$  km/s) for a period of about 8 h before the event described here. Both ACE and Wind satellites registered sudden increases in proton number density from 20 to 50  $\text{cm}^{-3}$ . A time lag of about 41 min for this increase in solar wind pressure to reach the magnetopause has been estimated using a method described in Lockwood et al. (2003), which uses both ACE and Wind positions at the time of the increase. Fig-

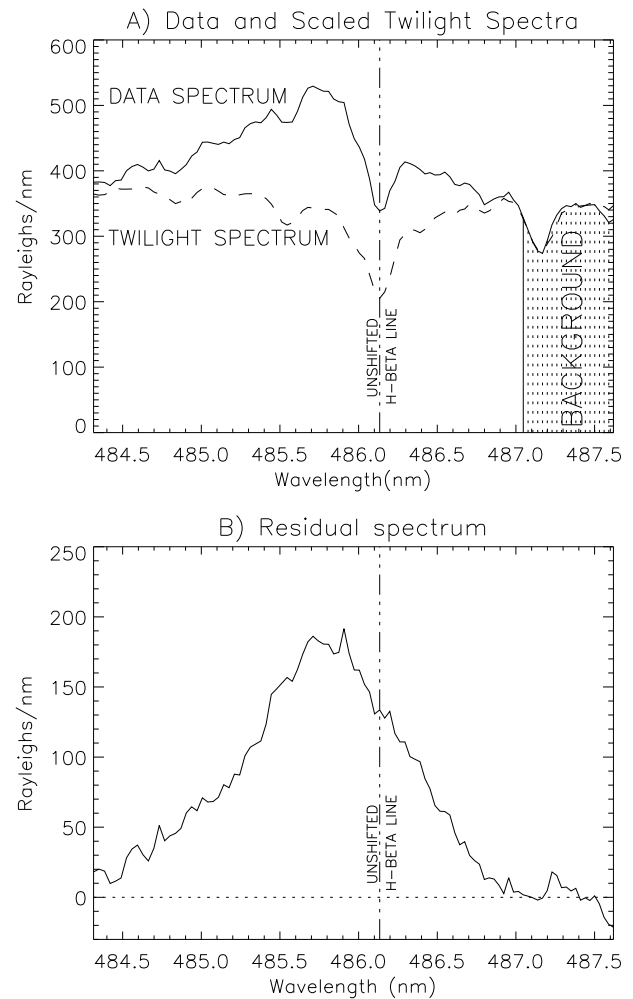


**Fig. 5.** (A) A measured spectrum (solid line), integrated for 60 s beginning at 09:21:57 UT on 27 November, 2000. The  $\phi$ -scaled twilight spectrum is drawn as a dashed line. (B) The residual spectrum after the scaled twilight spectrum has been subtracted from the data spectrum.

ure 7 is the ACE data lagged by this interval and plotted between 07:30–10:00 UT, which correspond to estimated times of arrival of the measured changes in solar wind parameters at the magnetopause. The density increase can be seen in the second panel at approximately 08:30 UT. The magnetic field components in Geocentric Solar Magnetospheric (GSM) coordinates are plotted in the lowest three panels. Following the density increase the magnetic field  $B_z$  changes from close to zero to positive ( $>20$  nT), and  $B_y$ , having been strongly positive (20 nT) at the time of the increase in solar wind pressure, subsequently becomes strongly negative ( $-20$  nT). At the same time  $B_z$  returns to almost zero. Three arrows mark the significant changes in the solar wind parameters which result in observable effects in the ionosphere.

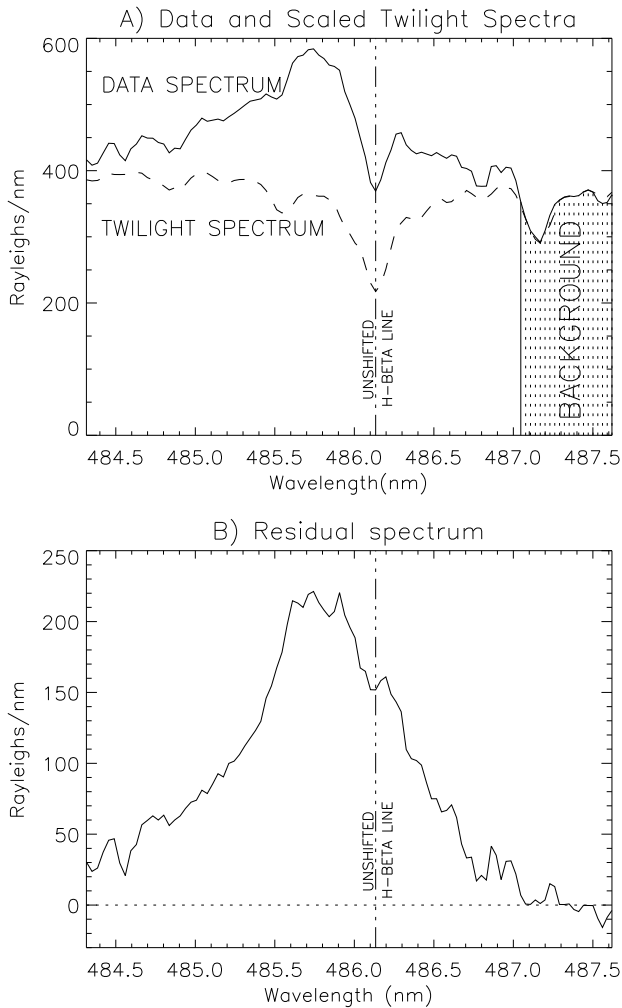


**Fig. 6.** (A) A measured spectrum (solid line), integrated for 60 s beginning at 09:25:22 UT on 27 November, 2000. The  $\phi$ -scaled twilight spectrum is drawn as a dashed line. (B) The residual spectrum after the scaled twilight spectrum has been subtracted from the data spectrum.

The IMAGE satellite was well located to provide an excellent overview of the large-scale changes in the auroral UV emissions related to the above changes in the solar wind. The first sign of the arrival of the pressure pulse generated by the increase in proton density is seen at 08:32:43 UT with a brightening of a region of Lyman- $\alpha$  emission centred at 14:30 MLT, in excellent agreement with the lag estimated and plotted in Fig. 7. This “spot” continues to fluctuate in intensity with a peak at 09:03:23 UT when it is centred closer to magnetic noon, but still duskward. During this time the oval is contracting poleward from an initially large area, resulting from earlier poleward  $B_z$ . By 09:32 UT the spot is centred at noon well poleward of the main oval and is over Svalbard. After this, the effect of the change in  $B_y$  is seen

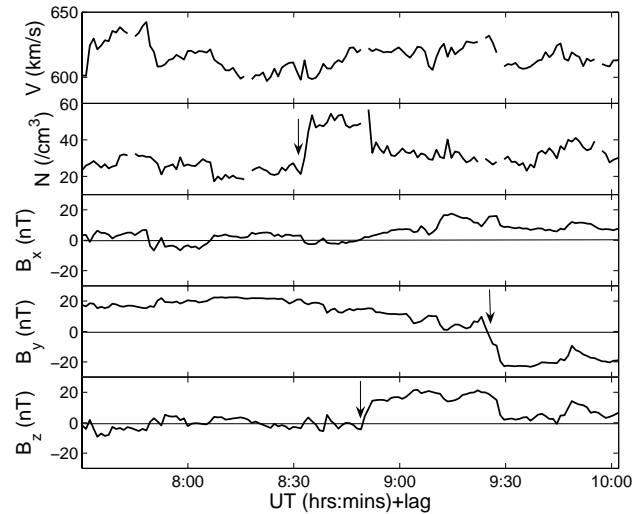


**Fig. 7.** Data from the ACE satellite for 27 November, 2000, lagged by 41 min. Arrows mark the times of significant changes that result in observed effects in the ionosphere.

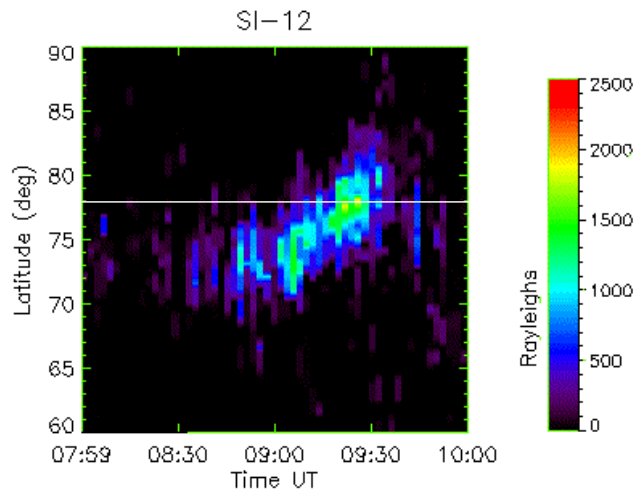


**Fig. 8.** Time history of IMAGE Lyman- $\alpha$  intensity at longitude of Longyearbyen. The horizontal line marks the latitude of Longyearbyen.

clearly as the spot moves downwards of noon, such that by 10:00 UT it is centred at 11:00 MLT (about 2 h MLT from Svalbard).

The spatial and temporal changes in Lyman- $\alpha$  brightness over Longyearbyen are shown in Fig. 8, which is a time sequence of latitude slices centred on longitude  $16.0^\circ$  and averaged over  $2^\circ$  in longitude. The geographic latitude of Longyearbyen is marked with a horizontal line. The figure confirms the presence of the intense proton aurora over Svalbard between 09:20 UT and 09:35 UT. Two Lyman- $\alpha$  images

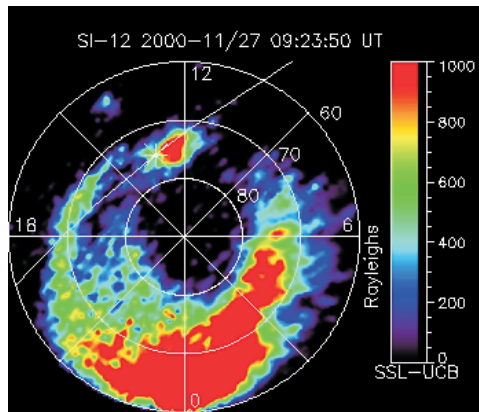


**Fig. 9.** IMAGE Lyman- $\alpha$  spectrograph data at 09:23:50 UT plotted in magnetic latitude and magnetic local time coordinates. The F12 footprint is drawn with a thin line and its position at this time is marked with an asterisk.

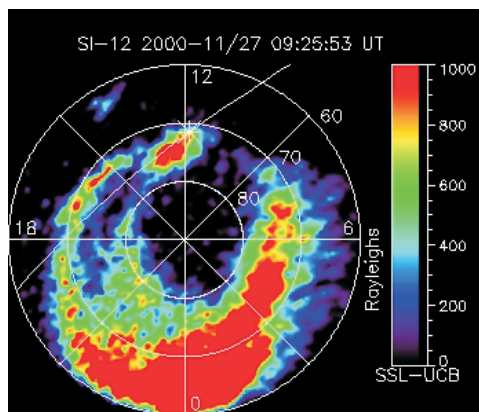


**Fig. 10.** As for Fig. 9 at 09:25:53 UT.

from the SI12 instrument at 09:23:50 UT and 09:25:53 UT, at the peak brightness of the event measured from the ground, are shown in Figs. 9 and 10. They also show the position of the DMSP F12 satellite as it crossed the region. Particle data from this pass are used in Sect. 4. At these times the cusp spot is still centred on the duskward side of 12:00 MLT, with most intensity poleward of the main auroral oval.

### 3.2 Ground-based optical measurements

Sunlight contamination has been removed from the HiTIES  $H_{\beta}$  profiles for the interval between 08:00 UT and 10:00 UT, and these are shown as a time series in the bottom panel of Fig. 11. The integrated brightness over the whole  $H_{\beta}$  spectrum is shown in the top panel. Significant  $H_{\beta}$  emission was first observed soon after 08:30 UT and continued through local magnetic noon (08:48 UT). HiTIES sees the largest emissions between 09:18 UT and 09:35 UT, confirm-

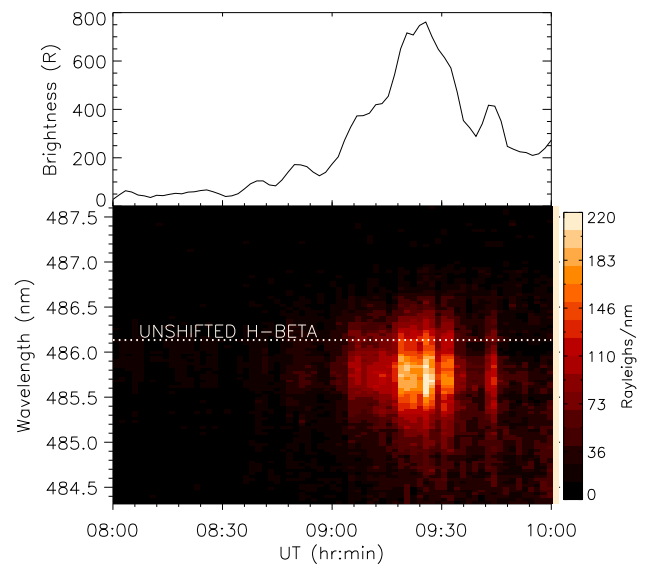


**Fig. 11.** (top) Changes in peak  $H_{\beta}$  intensity. (bottom) Changes in  $H_{\beta}$  profile intensities.

ing IMAGE/SI12 observations over Svalbard (Fig. 8). The solar contamination was already strong by 09:00 UT and by the end of the interval was two orders of magnitude larger than the  $H_{\beta}$  brightness. Three example plots are shown in Figs. 4–6 for the times 09:06 UT at the start of the event, and 09:22 UT and 09:25 UT. The Doppler shifted hydrogen profile is clearly present. The maximum integrated brightness of  $750 \pm 250$  R occurred at 09:25 UT. The short wavelength end of the spectra shows some variability which could be contaminating auroral emissions from the  $N_2$  Vegard-Kaplan (2,15) band. The effects of such emissions on the analysis are discussed in Sect. 4. The full analysis of the errors in the data from HiTIES can be found in Robertson (2006).

## 4 Modelling of $H_{\beta}$ profiles

In order to derive Doppler profiles of radiating hydrogen atoms, it is necessary to solve the equations for the transport of fast protons into the atmosphere, their energy degradation and scattering, and their conversion to neutral atoms. The present work adopts the Galand et al. (1998) model which takes into account the collisional angular redistribution through elastic collisions and through charge-changing collisions (i.e., capture and stripping). Starting with an incident proton beam, the resulting H emission Doppler profiles are determined from the computed particle intensities, neutral densities and emission cross-sections. Since the proton/H atom intensities in the upper atmosphere are directly proportional to the energy flux of the incident proton beam, the  $H_{\beta}$  Doppler profile is also proportional to the energy flux

of the incident proton beam. The detailed shape depends on the precipitating proton energy spectrum and pitch angle distribution. A full description of the model is given in Galand et al. (1998) and Lanchester et al. (2003). The latter contains examples of model results compared with HiTIES measured profiles and an appendix with a full description of the model equations.

At the time of the brightest feature measured over Longyearbyen there was a close passage of the DMSP F12 satellite. Its footprint and position at the times of two consecutive images are marked in Fig. 9 and Fig. 10, when Svalbard was directly beneath the cusp spot. As F12 travelled through the cusp region, the measured differential energy flux of protons (not shown) was increased for energies above 100 eV up to the maximum energy measured by the satellite of 30 keV. The electron differential energy flux was also increased for energies between 100 eV and 1 keV. Three ion energy spectra typical for the data acquired during the Svalbard overpass have been selected as input to the model. Above the cut-off energy of the DMSP ion spectrometer (30 keV) we have extrapolated the particle flux logarithmically to 100 keV in all three cases. For the ion data at 09:24:10 UT and 09:25:00 UT the input spectra have also been generated with a sharp cut-off at 30 keV for an estimation of the sensitivity of the  $H_{\beta}$  profiles to the high energy tail. These input spectra are shown in the top panel of Fig. 12. The energy flux  $Q_0$  and mean energy  $E_m$  in each case are:

time (UT)	shape	$Q_0$ ( $\text{mW m}^{-2}$ )	$E_m$ (keV)
09:24:10	extrapol 100 keV	1.6	2.7
09:24:10	sharp tail	1.2	2.0
09:24:30	extrapol 100 keV	2.8	3.0
09:25:00	extrapol 100 keV	3.2	4.0
09:25:00	sharp tail	2.2	2.8

The corresponding model profiles calculated along the magnetic zenith for the five input spectra are plotted in normalised form in the lower panel of Fig. 12. The instrument spectral resolution of 0.13 nm has been convolved with the model results. It can be seen that the high energy tail has a small effect on the short wavelength wing of the profiles, with the most raised wing corresponding to the logarithmically extrapolated spectrum at 09:25:00 UT. A distinct effect is seen in the shape of the profiles for input spectra with larger fluxes around 1–10 keV, most evident in the 09:24:30 UT spectrum. This results in a broadening of the  $H_{\beta}$  profile around 485.5 nm.

The model profile resulting from the F12 input spectrum at 09:25 UT has been chosen for comparison with four profiles measured between 09:22–09:26 UT in Fig. 13. The model profile (thick dashed line) is scaled to fit approximately to the

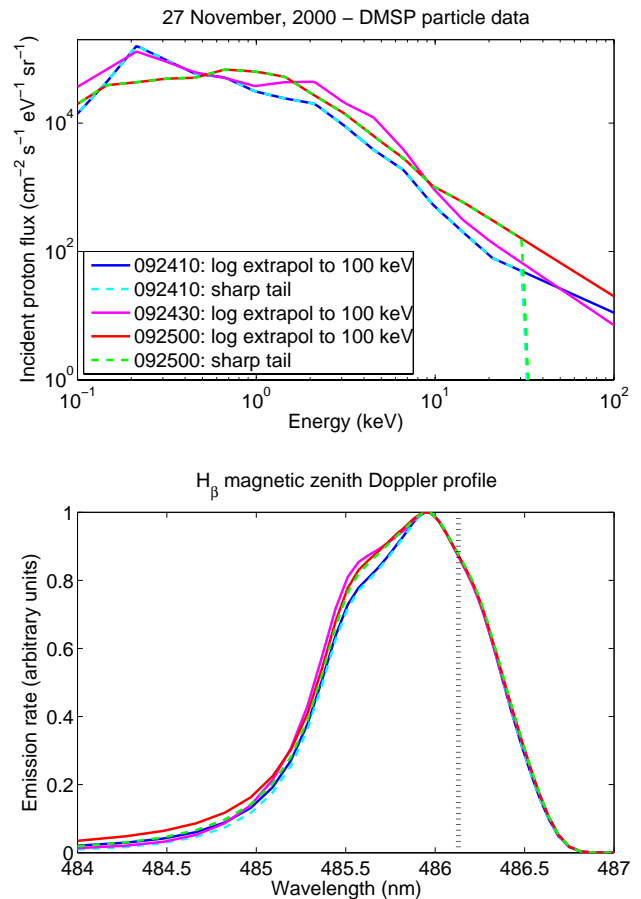


**Fig. 12.** (top) DMSP F12 input ion fluxes with and without high energy extrapolation. (bottom) Doppler-shifted  $H_{\beta}$  profiles along the magnetic zenith resulting from the  $H^+/H$  model driven by the DMSP input spectra above.

peak of the measured profiles. The overall shapes of both the modelled and the observed  $H_{\beta}$  Doppler profiles are similar. The solar subtraction appears to be very slightly overdone, such that there is a dip in the long wavelength or “red” wing of the profile corresponding to the position of the Fraunhofer absorption line. The main difference is in the raised short wavelength or “blue” wing, which is underestimated by the model results. This underestimation is not surprising as it corresponds to an underestimation of the energy spectra above the DMSP energy cut-off. As the observed  $H_{\beta}$  emission event is associated with a significant pressure pulse, it is very probable that protons of high energy (above 30 keV) have flux larger than usual. As mentioned above, there may be electron induced auroral emission from the  $N_2$  VK band. There is no way currently of estimating the extent of such emission during twilight hours, but it could have the effect of increasing the background to be subtracted at short wavelengths, and therefore reducing the height of the measured blue wing. The blue wing may also be affected

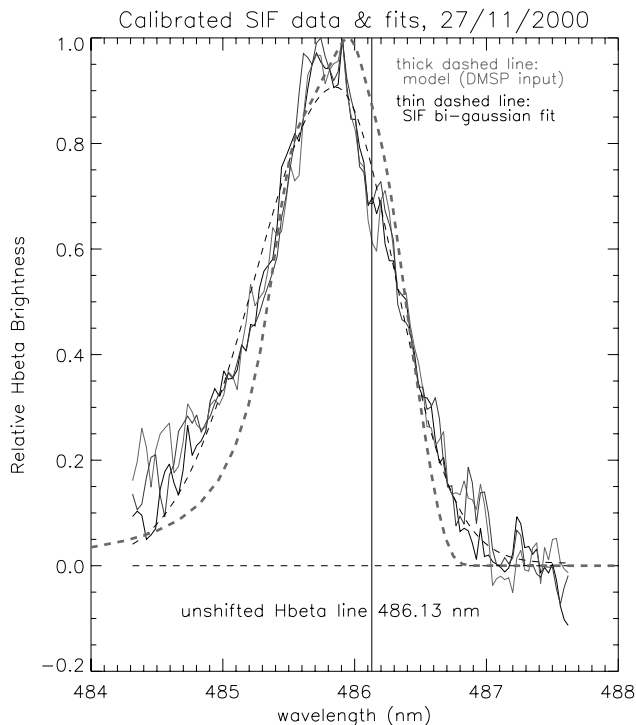


**Fig. 13.** Comparison of measured (solid lines) and modelled (thick dash)  $H_{\beta}$  profiles. The thin dashed line is a fit to the measured profiles.

by the presence of patchy cloud, which would scatter  $H_{\beta}$  into the detector from other parts of the sky, producing a more symmetric profile. Also, if a background measurement had been possible shortward in wavelength of the H emission profile, this may have reduced the blue wing further. Different mosaic filters have subsequently been designed for HiTIES that make this a possibility in future daytime measurements. While the comparison of the modelled profiles with the HiTIES data is limited above 30 keV due to the lack of particle data at the top of the atmosphere, the comparison with the model confirms the shape of the profiles below this energy. The model results have previously been validated against observed  $H_{\beta}$  profiles of proton aurora in dark sky conditions (Lanchester et al., 2003; Ivchenko et al., 2004).

## 5 Discussion

Changes in the brightness and position of hydrogen emissions in the region of the cusp reveal much about the reconnection processes which allow protons to precipitate into the high latitude ionosphere. For the events of 27 November 2000, described here, there was a particularly high density of protons in the solar wind, following a string of halo CMEs a few days before. From the lagged solar wind measurements shown in Fig. 7 it can be seen that an increase in proton density was estimated to arrive at the magnetopause just after

08:30 UT. The lag can only be estimated to within  $\pm 3$  min; the arrival of the pressure pulse is clearly seen at 08:33 UT on the ground by HiTIES, and by the IMAGE spectrographs, confirming that the plotted lag of 41 min is a good prediction. At this time the IMF was almost entirely in the positive  $B_y$  direction. The reconnection site under this condition is predicted to be at high latitudes on the dusk side of noon in the northern hemisphere for anti-parallel reconnection (Crooker, 1979; Luhmann et al., 1984; Chisham et al., 2002). Both the SI12 Lyman- $\alpha$  measurements as well as those from the SI13 imager confirm that precipitation has occurred in the post-noon sector, with increased brightness of emissions. The latter are associated predominantly with OI 135.6 nm oxygen emission, which could be either from primary precipitating electrons, or indirectly from secondary electrons produced by protons and hydrogen atoms as they precipitated. The F12 electron energy spectra confirm that there were indeed precipitating electrons in the energy range 100 eV to 1 keV in this region. The study of the relative importance of protons and electrons in such a reconnection event is an important subject, but it is not addressed further here. Analysis of the large-scale hydrogen and electron aurora and associated ionospheric flows during this interval will be presented in a separate paper.

Before the arrival of the pressure pulse and its manifestation as a bright spot duskward of noon, the auroral oval was particularly large, following a time of negative  $B_z$ . The proton spot appears first within the main oval. As the IMF  $B_z$  increases, the spot brightens and is seen poleward of the oval and closer to noon at 08:47 UT. The oval contracts steadily thereafter during the period of positive  $B_z$  and a steady decrease of  $B_y$  to zero. The next effect that is seen is the sudden change to purely negative  $B_y$ , during which time the spot moves rapidly to pre-noon. These changes correspond to the reconnection site moving through higher latitudes across the noon meridian (when the IMF was in positive  $B_z$  direction), to the opposite lobe on the pre-noon magnetopause. The longitudinal shift of the cusp may be enhanced by the distortion of magnetospheric field lines by IMF  $B_y$  (Cowley et al., 1991). The changes in latitude of the spot in Lyman- $\alpha$  can be seen over Svalbard in Fig. 8. At the start of the interval, the oval is south of Svalbard, and the first significant increase in brightness is seen at about 73° N geographic latitude just after 08:30 UT. The contraction of the oval follows, with the brightest and most northerly emissions seen at 09:25 UT over Svalbard at 78° N latitude, corresponding to the time of maximum  $B_z$ . After that the spot moves away to pre-noon and Svalbard also rotates even further way from noon in the opposite sense. The region of emission moves slightly equatorward again as the IMF  $B_z$  returns to zero. This behaviour of the cusp spot is consistent with previous studies, for example Milan et al. (2000), who used FUV measurements from the Polar satellite to study the response of dayside emissions to changes in IMF direction, during predominantly northward IMF.

From the ground, measurements of  $H_{\beta}$  Doppler profiles provide information about the changes to the energy of the incoming protons. We use a simple fitting process to estimate the changes in the shape and in the peak brightness and wavelength of the peak. The method is described fully by Lummerzheim and Galand (2001). A synthetic line profile is constructed from a Gaussian shape with different half widths on the short and long wavelength sides of the peak, thus accounting for the different Doppler shift produced by precipitation towards the instrument and scattering of hydrogen away from the instrument, respectively. These synthetic spectra are fitted to the measured profiles, using a nonlinear least squares fitting method. A sample fitted profile is drawn as a thin dashed line in Fig. 13. The changes in blue wing halfwidth and peak wavelength (not shown) are not large, although there is a slight trend to larger blue shift with time between 09:05 and 09:35 UT. Previous results (Lanchester et al., 2003) from the afternoon oval have found that changes in the blue wing correspond to changing energy distributions associated with the large scale movement of the proton precipitation region over the ground station. The blue wing halfwidth of these previous measurements from Longyearbyen range between 0.6 and 1.0 nm, extending higher than but overlapping with the values measured here (0.6–0.8 nm), whereas those measured at lower latitudes (in the afternoon/evening sector of the auroral oval) have been found to have a greater blue wing extent of up to 2.0 nm (Galand et al. (2004) and references therein). There is no strong evidence here of a velocity filter in operation as described in Deehr et al. (1998). Their observation coincided with an equatorward motion of the dayside aurora, and therefore was the result of different processes from those observed here, where the brightest emissions occur at a time of northward IMF, and the subsequent combination of a sudden change in IMF  $B_y$  and the rotation of the earth moved the cusp precipitation abruptly away from our ground station. Careful consideration of spatial and temporal changes is crucial when interpreting ground-based data. Here the motion of the emission region relative to Svalbard is a mixture of changes in both latitude and longitude, which makes interpretation of the event complicated.

## 6 Summary

The purpose of this paper is to demonstrate that  $H_{\beta}$  profiles measured during twilight hours can be used in the study of cusp daytime precipitation. The profiles have been extracted from data that would normally have been rejected because of the contamination from scattered sunlight. The fortuitous pass of the DMSP F12 satellite on 27 November 2000, coincided with the time that the  $B_y$  component of the IMF was changing from strongly positive to strongly negative, and thus just as the proton induced auroral spot was about to move to its pre-noon position. It also coincided with the

time of brightest  $H_{\beta}$  measured at Svalbard. The ion energy spectra measured by F12 are therefore very suitable as input for modelling. The comparison of modelled profiles with the data is limited by the low energy cut-off of the ion detector (30 keV). The high energy ion spectral tail has been extrapolated logarithmically up to 100 keV, which is a plausible guess but remains arbitrary. Closer fits of the model to the data at large blue shifts could possibly be made by changing the high energy tail. The comparison is also limited by uncertainties in differential cross sections. The width of the spectrum at half maximum fits well, but it can be seen from the different model results that small variations will occur with changes to the energy flux and mean energy in this region. Although the F12 satellite passed close to Longyearbyen, it did not pass exactly over the ground site, so differences in this region of the profile would be expected. There is evidence that the background subtraction could be refined still further, if the effect of electron auroral emissions can be estimated, and with the inclusion of background subtraction from the short wavelength end of the spectrum.

We were also fortunate to have data from IMAGE with which to compare the ground-based measurements. These confirm that the cusp precipitation resulted from the observed changes in the IMF. In future, using this technique,  $H_{\beta}$  profiles during daytime can be used to reveal the signature of proton precipitation, and therefore extract information about the energy flux and mean energy of the protons by comparing the profiles with model results. No clear dispersion signature was observed in the cusp protons, but this is not surprising given the sudden movement of the cusp emission region away from Svalbard at the time of maximum intensity. This combination of ground-based measurements and modelling provides a method of detecting changes in energy that result from dayside reconnection, both at low latitudes (Deehr et al., 1998), and in the high latitude lobe regions as seen here. The use of more than one spectrograph on the ground in the cusp would be of great benefit to this study as suggested by Deehr et al. (1998).

*Acknowledgements.* The DMSP particle detectors were designed by D. Hardy of AFRL, and data obtained from JHU/APL. The authors thank D. Hardy, F. Rich and P. Newell for its use, and in particular F. Rich for providing data specific to our needs. ACE and Wind data were obtained from CDAWeb and we acknowledge the following PIs: D. J. McComas, R. Lepping and K. Ogilvie. Thanks are offered to H. Frey for supplying the IMAGE data and for help with data reduction. The research was supported by the PPARC in the UK which also funded the spectrograph. M. Galand was supported in part by NASA grant NAG5-12773, D. Lummerzheim by NASA grants NAG5-11694 and NAG5-12192. We acknowledge with gratitude the help given in this work by the late N. Shumilov.

Topical Editor M. Pinnock thanks C. Deehr and B. V. Kozelov for their help in evaluating this paper.

## References

- Baumgardner, J., Flynn, B., and Mendillo, M.: Monochromatic imaging instrumentation for applications in aeronomy of the earth and planets, *Optical Eng.*, 32, 3028–3032, 1993.
- Chakrabarti, S., Pallamraju, D., Baumgardner, J., and Vaillancourt, J.: HiTIES: A High Throughput Imaging Echelle Spectrograph for ground-based visible airglow and auroral studies, *J. Geophys. Res.*, 106, 30 337–30 348, 2001.
- Chisham, G., Pinnock, M., Coleman, I. J., Hairston, M. R., and Walker, A. D. M.: An unusual geometry of the ionospheric signature of the cusp: implications for magnetopause merging sites, *Ann. Geophys.*, 20, 29–40, 2002, <http://www.ann-geophys.net/20/29/2002/>.
- Cowley, S. W. H., Morelli, J. P., and Lockwood, M.: Dependence of convective flows and particle precipitation in the high-latitude dayside ionosphere on the X and Y components of the interplanetary magnetic field, *J. Geophys. Res.*, 96, 5557–5564, 1991.
- Crooker, N. U.: Dayside merging and cusp geometry, *J. Geophys. Res.*, 84, 951–959, 1979.
- Deehr, C. S., Lorentzen, D. A., Sigernes, F., and Smith, R. W.: Dayside auroral hydrogen emission as an aeronomic signature of magnetospheric boundary layer processes, *Geophys. Res. Lett.*, 25, 2111–2114, 1998.
- Frey, H. U., Mende, S. B., Immel, T. J., Fuselier, S. A., Clafin, E. S., Gerard, J.-C., and Hubert, B.: Proton aurora in the cusp, *J. Geophys. Res.*, 107, A7, doi:10.1029/2001JA900161, 2002.
- Galand, M., Lilienstein, J., Kofman, W., and Lummerzheim, D.: Proton transport model in the ionosphere: 2, Influence of magnetic mirroring and collisions on the angular redistribution in a proton beam, *Ann. Geophys.*, 16, 1308–1321, 1998, <http://www.ann-geophys.net/16/1308/1998/>.
- Galand, M., Baumgardner, J., Pallamraju, D., Chakrabarti, S., Lovhaug, U. P., Lummerzheim, D., Lanchester, B. S., and Rees, M. H.: Spectral imaging of proton aurora and twilight at Tromsø, Norway, *J. Geophys. Res.*, 109(A7), A07305, doi:10.1029/2003JA010033, 2004.
- Galand, M. and Chakrabarti, S.: Proton aurora observed from the ground, *J. Atmos. Ter. Phys.*, 68, 1488–1501, 2006.
- Henriksen, K., Fedorova, N. I., Totunova, G. F., Deehr, C. S., Romick, G. J., and Sivjee, G. G.: Hydrogen emissions in the polar cleft, *J. Atmospheric Terr. Phys.*, 47, 1051–1056, 1985.
- Ivchenko, N., Galand, M., Lanchester, B. S., Rees, M. H., Lummerzheim, D., Furniss, I., and Fordham, J.: Observation of  $O^+(^4P-^4D^0)$  lines in proton aurora over Svalbard, *Geophys. Res. Lett.*, 31, L10807, doi:10.1029/2003GL019313, 2004.
- Lanchester, B. S., Galand, M., Robertson, S. C., Rees, M. H., Lummerzheim, D., Furniss, I., Peticolas, L. M., Frey, H. U., Baumgardner, J., and Mendillo, M.: High resolution measurements and modelling of auroral hydrogen emission line profiles, *Ann. Geophys.*, 21, 1629–1643, 2003, <http://www.ann-geophys.net/21/1629/2003/>.
- Lockwood, M., Lanchester, B. S., Frey, H., Throp, K., Morley, S., Milan, S. E., and Lester, M.: IMF Control of Cusp Proton Emission Intensity and Dayside Convection: implications for component and anti-parallel reconnection, *Ann. Geophys.*, 21, 955–982, 2003, <http://www.ann-geophys.net/21/955/2003/>.
- Lorentzen, D. A., Sigernes, F., and Deehr, C. S.: Modeling and observations of dayside auroral hydrogen emission Doppler profiles, *J. Geophys. Res.*, 103, 17 479–17 488, 1998.
- Luhmann, J. G., Walker, R. J., Russell, C. T., Crooker, N. U., Spreiter, J. R., and Stahara, S. S.: Patterns of potential magnetic field merging sites on the dayside magnetopause, *J. Geophys. Res.*, 89, 1739–1742, 1984.
- Lummerzheim, D. and Galand, M.: The profile of the hydrogen  $H\beta$  emission line in proton aurora, *J. Geophys. Res.*, 106, 23–31, 2001.
- Milan, S. E., Lester, M., Cowley, S. W. H., and Brittnacher, M.: Dayside convection and auroral morphology during an interval of northward interplanetary magnetic field, *Ann. Geophys.*, 18, 436–444, 2000, <http://www.ann-geophys.net/18/436/2000/>.
- McWhirter, I., Furniss, I., Aylward, A. D., Lanchester, B. S., Rees, M. H., Robertson, S. C., Baumgardner, J., and Mendillo, M.: A new spectrograph platform for auroral studies in Svalbard, *Proc. 28th Ann. Europ. Meeting of Atmospheric Studies by Optical Methods*, S.G.O. Publications, 92, 73–37, 2003.
- Mende, S. B.: Far ultraviolet imaging from the IMAGE spacecraft, *Space Sci. Rev.*, 91, 287–318, 2000.
- Robertson, S. C.: The characterisation of the High Throughput Imaging Echelle Spectrograph and Investigations of Hydrogen  $\beta$  Emission over Svalbard, PhD thesis, University of Southampton, 2006.
- Sigernes, F., Lorentzen, D. A., Deehr, C. S., and Henriksen, K.: Calculation of auroral Balmer volume emission height profiles in the upper atmosphere, *J. Atmos. Terr. Phys.*, 56, 503–508, 1994.
- Sigernes, F.: Estimation of initial auroral proton energy fluxes from Doppler profiles, *J. Atmos. Terr. Phys.*, 58, 1871–1883, 1996.